International Journal of Precision Engineering and Manufacturing-Green Technology (2020) 7:595–607
https://doi.org/10.1007/s40684-019-00152-y

Online ISSN 2198-0810
Print ISSN 2288-6206

REGULAR PAPER

# Integration of Forming Operations on Hybrid Additive Manufacturing Systems Based on Fusion Welding

João P. M. Pragana[1] · Valentino A. M. Cristino[2] · Ivo M. F. Bragança[1,3] · Carlos M. A. Silva[1] · Paulo A. F. Martins[1]

Received: 20 June 2019 / Revised: 19 August 2019 / Accepted: 20 August 2019 / Published online: 4 September 2019


## Abstract

This paper is focused on the integration of metal forming operations in hybrid systems that combine additive manufacturing (AM) by gas metal wire arc and subtractive manufacturing by machining. The investigation is carried out in AISI 316L stainless steel wire and draws from tensile testing to incremental sheet forming of truncated conical shapes. Commercial sheets from the same material are utilized for comparison purposes. Thickness measurements, digital image correlation (DIC), circle grid analysis (CGA) and microstructural and scanning electron microscopy (SEM) observations are carried out to understand how different is the mechanical behaviour of the deposited metal from that of commercial metal sheets and how significant is the influence of the deposited metal microstructure on its overall formability. Results confirm that integration of metal forming operations in hybrid AM routes is feasible despite the formability of deposited metal being smaller than that of the commercial metal sheets due to the strong anisotropy induced by the dendritic based microstructure of the deposited metal. Incremental forming of two deposited parts also allows concluding that integration of metal forming operations in hybrid AM systems is a step towards green and sustainable manufacturing by extending their field of applicability to the fabrication of complex ready-to-use parts requiring combination of different processes.

**Keywords** Additive manufacturing · Hybrid system · Multi-tasking · Formability · Stainless steel

## 1 Introduction

The last years have seen a growing interest in additive manufacturing (AM) due to its capability of operating beyond typical limitations of conventional manufacturing processes [1]. Although AM was originally developed for the fabrication of prototypes, it is currently utilized to produce fully dense parts for end-use applications in a wide variety of materials ranging from plastics and ceramics to metals [2].

In case of metals, AM may be classified into three main categories; powder bed fusion (PBF), direct writing (DW) and direct energy deposition (DED). PBF produces metal parts by slicing its geometry into layers and adding the individual particles of powder together one layer at a time on the build platform by means of a focused heat source. DW is based on the ejection and deposition of uniform molten metal-droplets onto a computer controlled moving build platform to produce metal parts with relatively low energy consumption. DED produces metal parts by pushing powder or wire through a feed nozzle where it is melted and added onto the build platform by means of a focused heat source.

✉ Paulo A. F. Martins
pmartins@tecnico.ulisboa.pt

João P. M. Pragana
joao.pragana@tecnico.ulisboa.pt

Valentino A. M. Cristino
vcristino@um.edu.mo

Ivo M. F. Bragança
ibraganca@dem.isel.ipl.pt

Carlos M. A. Silva
carlos.alves.silva@tecnico.ulisboa.pt

1 IDMEC, Instituto Superior Técnico, Universidade de Lisboa, Av. Rovisco Pais, 1049-001 Lisbon, Portugal

2 Department of Electromechanical Engineering, University of Macau, Avenida da Universidade, Taipa, Macao, China

3 ISEL, GI-MOSM, Instituto Superior de Engenharia de Lisboa, Instituto Politécnico de Lisboa, Rua Conselheiro Emídio Navarro, 1959-007 Lisbon, Portugal

PBF is mostly suitable for complex metal parts where geometrical precision and surface finishing is a concern due to its capability to produce near-net shapes with little post-processing requirements by means of secondary machining operations. Because metal powder is spread on the build platform and then selectively fused, PBF has a tendency of leaving a significant amount of unfused powder that can be subsequently reutilized.

DW has been mainly utilised for producing flexible circuits and advanced electronic components but recent advances in piezoelectric [3] and pneumatic [4] pulse systems seem promising for producing small thin-walled metal parts because they can produce a thin shell utilizing several layers of droplets only.

DED can produce larger metal parts at much higher build rates than PBF [5]. Material usage in DED is very efficient in situations where only the required amount of material is deposited onto the build platform. However, in ordinary situations where post-processing through machining operations is required, additional material and energy consumption combined with the increase of process lead time generally have a negative impact on the overall manufacturing costs [6]. Recent studies focused on the sustainability of AM show that inefficient use of the technology may lead to specific energy consumptions up to 100 times higher than those of conventional mass production technologies [7, 8].

The integration of DED into machining centres (with milling and/or turning capabilities) to create hybrid systems that combine additive and subtractive manufacturing is an effective solution to minimize some of the above-mentioned difficulties regarding the production of ready-to-use metal parts in smaller production lead times [9, 10]. The possibility of combining additive and subtractive manufacturing in one machine using a single clamping shortens the overall processing time and ensures higher accuracies in the production of complex ready-to-use parts [1].

Nowadays, the concept of hybrid systems is being extended to the possibility of combining additive and subtractive manufacturing with metal forming stages aimed at changing the shape and alter the surface of metal parts while keeping its volume constant (Fig. 1).

In a recent patent, Tekkaya et al. [11] proposed the integration of sheet metal forming, laser powder deposition and surface finishing in a single hybrid system [9]. The rationale behind the integration of metal forming in hybrid AM systems is to foster its development and usage in mass customization [12]. Typical examples involve material deposition on metal parts fabricated by bending [6], deep drawing [13] and single point incremental forming [14] to locally improve strength and wear resistance, among other benefits.

However, the inverse processing route is also start being investigated, meaning that AM is now being considered to produce pre-forms for subsequent metal forming stages. The deposition of stiffness reinforcements in metal parts for subsequent forming operations [7, 15, 16] and the deposition of tenons [17] in sheets for applications in joining by forming are two examples of this new processing route.

Despite the advances in hybrid AM systems, it is important not to forget that available DED technology based on laser heat sources is still very expensive. This problem has been stimulating researchers to the development and use of alternative, affordable DED technologies, based on fusing welding. The resulting systems are built upon the integration of gas metal arc, gas tungsten arc or plasma welding equipment into CNC mechanisms to deposit metal in the desired regions [18].

The willingness to implement these alternative AM solutions in the industry is strong as companies already own the welding equipment and can easily buy or build the required

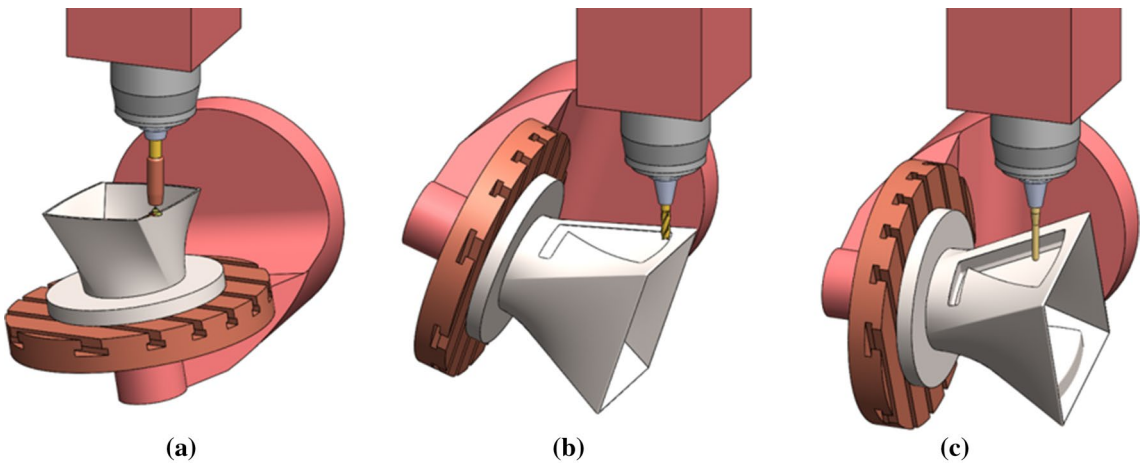


**Fig. 1** Schematic representation of a hybrid multi-tasking processing route comprising **a** metal deposition, **b** milling and **c** forming

CNC mechanisms. Moreover, the combination of AM based in gas metal wire arc (also designated as wire arc additive manufacturing—WAAM) with subtractive manufacturing enables significant material and energy savings with respect to conventional fabrication processes [19]. WAAM based systems are also more efficient than laser-based systems due to its higher deposition rates and to the large energy requirements of powder-based heat sources to turn electrical energy into laser power [20].

However, DED technologies, based on fusing welding, still have difficulties and limitations to be integrated with metal forming in hybrid multi-tasking systems aimed at producing ready-to-use metal parts. Major problems are originated by the microstructure and processing defects resulting from metal deposition, which may limit the capability to withstand large plastic deformations of metal forming.

Studies focused on the overall formability [21, 22], anisotropy [23] and residual stresses originated by the heating–cooling cycles [24] of metal forming are currently undergoing to provide answers to the following basic questions: (i) how different is the mechanical behaviour of the deposited metal from that of a commercial rough metal? and (ii) how significant is the influence of the deposited metal microstructure on formability?

This paper is focused on providing answers to these questions and employs a hybrid multi-tasking processing route comprising WAAM, milling and incremental sheet metal forming to investigate the feasibility of producing truncated conical shapes from deposited AISI 316L stainless steel (Fig. 1). Results from conventional incremental forming of commercial AISI 316L sheets are included for comparison purposes.

The fabrication of a complex truncated eight-lobe conical shape is also included to illustrate the benefits of employing the proposed hybrid AM systems containing additive, subtractive and forming manufacturing stages against existing AM systems solely having additive and subtractive capabilities, and against conventional incremental forming of commercial sheets that would inevitable require the utilization of jigs with dedicated blank holders and backing plates.

## 2 Experimentation

### 2.1 Deposited Material and Mechanical Characterization

Metal deposition was carried out in a 3-axis CNC system equipped with a gas metal arc welding machine LUC 400 Aristo 400 from ESAB. An AISI 316L stainless steel wire with 1 mm diameter was pushed through the welding torch and subsequently melted and added on 260 × 70 × 15 mm hot-rolled AISI 316L baseplates. The shielding gas was 99.9% of Argon and the major parameters utilized in metal deposition are given in Table 1.

The AISI 316L stainless steel was deposited one layer at a time onto the baseplate (Fig. 2a) with a single bead by a welding torch that was programmed with a reciprocate movement and a working angle of 90º (Fig. 2b). The resulting as-built parts had ‘U-shaped’ geometries with 265 mm

**Table 1** Metal deposition parameters utilized in WAAM

| Current (A) | Voltage (V) | Wire feed speed (m/min) | Welding speed (mm/min) | Stick-out length (mm) | Gas flow rate (l/min) | Bead height (mm) |
|---|---|---|---|---|---|---|
| 100 | 16.5 | 6 | 600 | 8–12 | 10 | 1.8 |

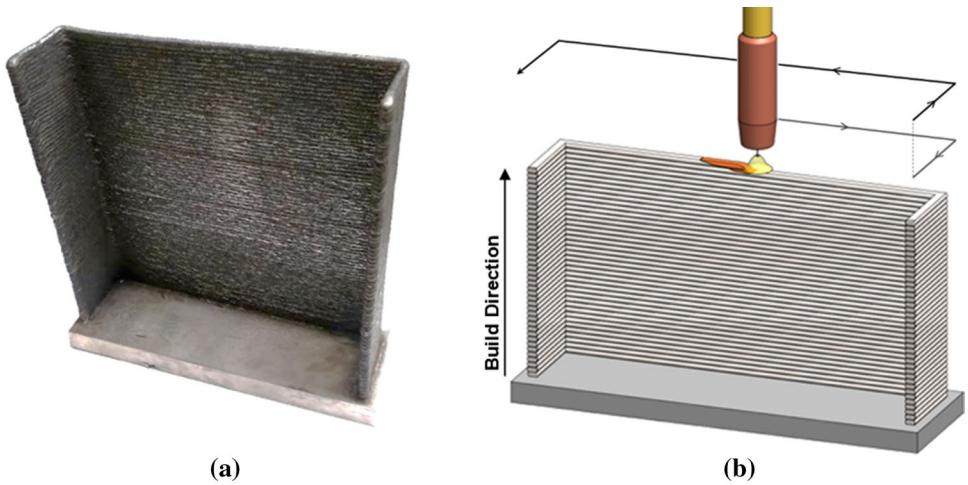


**Fig. 2** AISI 316L stainless steel deposited by WAAM. **a** Photograph of the as-build U-shaped part; **b** Schematic representation of the reciprocate deposition strategy

length, 225 mm height and 50 mm side wall width. The single bead layers were approximately 4 mm thickness.

The mechanical characterization of the deposited AISI 316L stainless steel at room temperature was carried out by means of tensile tests on an INSTRON 5900 universal testing machine. The tests followed the ASTM standard E8/E8 M-16 [25] and the specimens were cut out from the deposited U-shaped parts by water jet at 0º, 45º and 90º with respect to the build direction (Fig. 3a). Milling after deposition was needed to extract tensile test specimens with the required thickness and surface conditions.

The different locations from where the specimens were cut out allowed characterizing anisotropy and understanding the stress–strain behaviour of the deposited material with respect to the build direction (Fig. 3a).

The formability of the deposited test specimens was analysed by means of digital image correlation (DIC). For this purpose, the surfaces of their reduced sections were sprayed with a stochastic black speckle pattern on a uniform background previously painted in white (Fig. 3b).

The DIC system utilized by the authors was from Dantec Dynamics (model Q-400 3D) and was equipped with two cameras with a resolution of 6 megapixels and 50.2 mm focal lenses with an aperture of f/11. The measuring region was illuminated by a spotlight and the images were acquired with a frequency of 20 frames per second. The analysis was performed with the INSTRA 4D from Dantec Dynamics, and a facet size of 13 pixels with a grid spacing of 7 pixels was considered for the correlation algorithm.

## 2.2 Integration of Forming in Hybrid AM Systems

Incremental sheet forming was utilized as a benchmark process to assess the integration of forming operations in hybrid AM systems containing additive and subtractive manufacturing (Fig. 4). The choice of incremental sheet forming was due to its well-known ability to plastically deform sheets to their limits of formability and thickness reduction [26].

Preparation of the deposited U-shaped part to incremental forming required post-processing by milling to simultaneously ensure good surface conditions and a uniform thickness of approximately 1 mm.

The U-shaped geometry was chosen to replicate working conditions in thin-walled hollow parts and to minimize distortion induced by the heating–cooling cycles of WAAM. In addition, and as will be seen later in results and discussion, the U-shaped geometry also avoids the use of blank holders and backing plates (Fig. 4a), which are mandatory in conventional incremental forming of metal sheets (Fig. 4b). Results obtained with commercial AISI 316L sheets are included in the paper for comparison purposes.

Strain grid analysis [27] was carried out in both deposited and commercial sheets to determine the strain loading paths and the strains at the onset of fracture. The experimental procedure involved electrochemical etching a grid of circles with 2.5 mm of initial diameter on the surfaces before deformation and measuring the major and minor in-plane strains by means of a computerised digital camera measuring system (GPA-100 model from ASAME) (Fig. 4c).

## 2.3 Microstructure and Fractography

The microstructure of the deposited U-shaped parts was analysed with an optical metallographic microscope (Motic model BA310 MET-H). For this purpose, metallographic samples were extracted from the parts and subsequently cleaned and ground with a series of SiC paper up to 1000 grit. Polishing was then conducted with 6 µm and 1 µm diamond suspensions

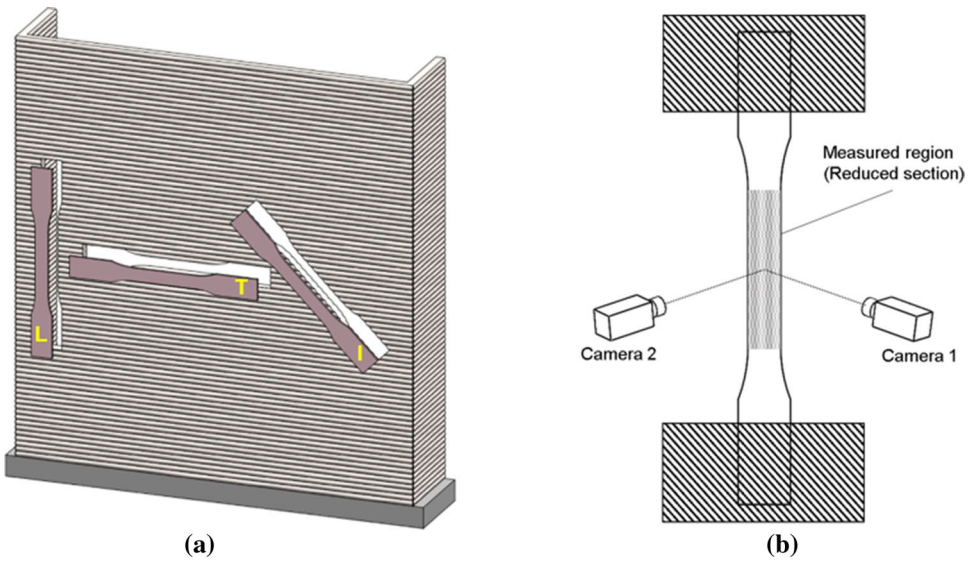


**Fig. 3** Mechanical characterization of the deposited AISI 316L stainless steel. **a** Regions of the U-shaped part from where the tensile test specimens were extracted; **b** Schematic representation of the digital image correlation system (DIC) that was utilized for measuring the in-plane strains during tensile tests

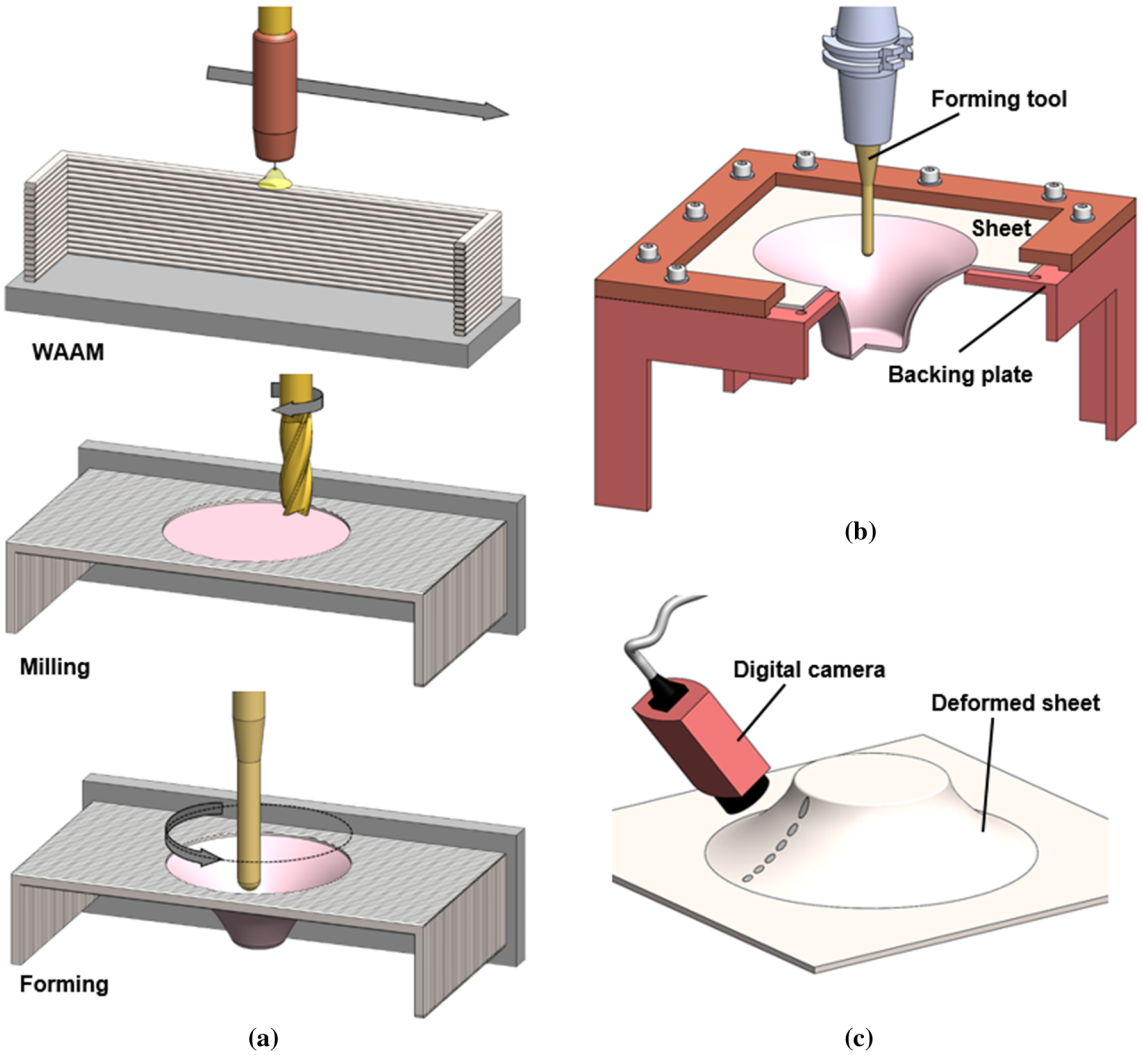


**Fig. 4** Process route to fabricate a truncated conical shape. **a** Integration of incremental sheet forming in a hybrid system equipped with additive (WAAM) and subtractive (milling) manufacturing; **b** Conventional incremental forming of a commercial metal sheet; **c** Schematic representation of the computerised digital camera measuring system for determining the strains

before subjecting the metallographic samples to electrochemical etching by immersion in chromic acid under a voltage of 9 V in order to reveal the grain boundaries.

The fracture surfaces of the incrementally formed parts made from deposited and commercial sheets were analysed in a Hitachi S-2400 scanning electron microscope (SEM) with the objective of characterizing its morphology and determining the crack opening modes.

## 3 Results and Discussion

### 3.1 Mechanical Behaviour and Formability of the Deposited Material

Figure 5 provides the stress–strain curves of the deposited AISI 316L stainless steel. The curves were obtained from

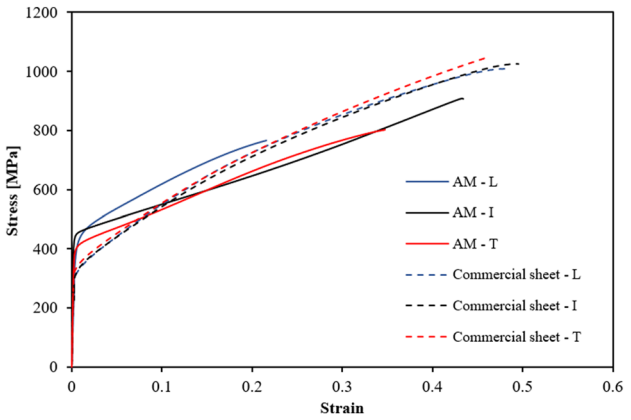


**Fig. 5** True stress–true strain curves of deposited (AM) AISI 316L stainless steel obtained from longitudinal (L), inclined (I) and transverse (T) test specimens with respect to the build direction. The reference direction for the commercial AISI 316L sheets in the rolling direction

**Table 2** Mechanical properties and anisotropy of the deposited and commercial AISI 316L

| Test specimens | Orientation | Yield stress (MPa) | Anisotropy, r |
|---|---|---|---|
| Deposited AISI 316L | L | 394 | 0.65–0.80 |
| | I | 440 | 0–0.03 |
| | T | 394 | 1.38–3.42 |
| Commercial AISI 316L | L | 325 | 0.94 |
| | I | 309 | 0.97 |
| | T | 306 | 0.84 |

tensile tests performed on longitudinal (L), inclined (I) and transverse (T) test specimens extracted from the U-shaped part at 0º, 45º and 90º with respect to the build direction (Fig. 3a). Stress–strain curves for test specimens extracted from commercial AISI 316L sheets at 0º(L), 45º(I) and 90º(T) degrees with respect to the rolling direction are included for comparison purposes.

Three main conclusions arise from these tensile tests. Firstly, the results included in Fig. 5 show different stress–strain evolutions for the longitudinal (L), inclined (I) and transverse (T) test specimens that were extracted from the deposited AISI 316L stainless steel (refer to 'AM' in the legend of Fig. 5). In particular, the stress and strain at fracture of the inclined test specimens are significantly larger than those of the longitudinal test specimens, which provide the lowest values of all. This means that the deposited metal is anisotropic, as can be further confirmed by the anisotropy coefficients that are included in Table 2. Moreover, the variation range of the anisotropy coefficients included in Table 2 reveals that not only the values are different for each direction of the deposited AISI 316L as they change from the beginning to the end of tensile tests.

Secondly, the largest stress and strain of the deposited material at fracture are smaller than those obtained for the commercial AISI 316L sheets, which are included in the figure for comparison purposes.

Thirdly, the yield stress of the deposited material is identical for all directions and higher than that of the commercial AISI 316L sheets (Table 2).

The above-mentioned mechanical behaviour of the deposited AISI 316L stainless steel is attributed to the microstructure of the U-shaped parts. In fact, the microstructure is characterized by dendrites with primary arms aligned with the build direction as a result of the significant temperature

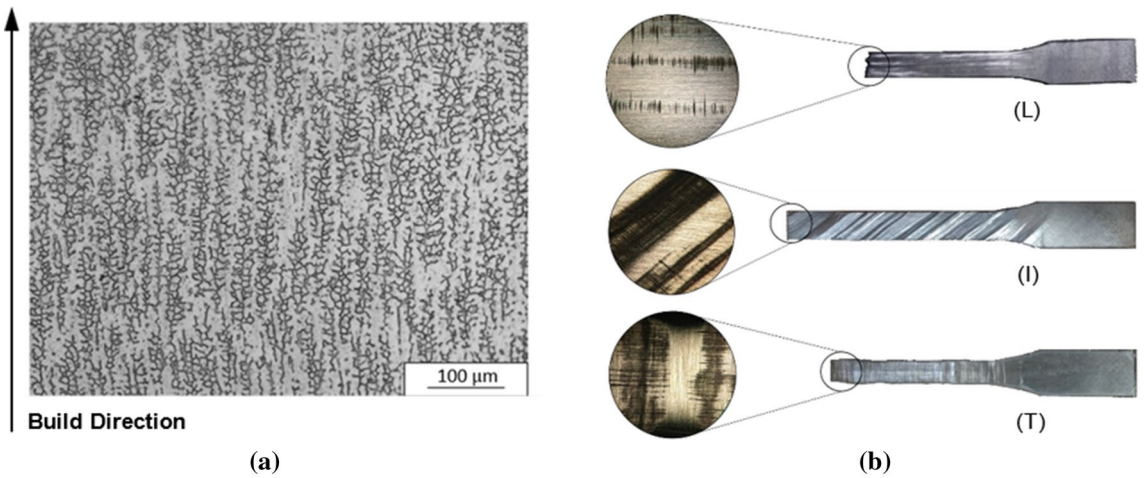


**Fig. 6** Microstructure of the tensile test specimens extracted from the deposited U-shaped part. **a** Optical micrograph of a metallographic sample extracted from the part; **b** Orientation of the primary arms of the dendrites in the longitudinal (L), inclined (I) and transverse (T) test specimens

gradient perpendicular to the reciprocated single bead layers (Fig. 6a). This type of microstructure, which is different from that observed in the commercial AISI 316L sheets, had already been identified by other authors [28] and is responsible for the anisotropic behaviour of the deposited U-shaped part (Fig. 6b).

Utilization of DIC during tensile tests allowed concluding that in case the loading direction is aligned with the inclined (I) or transverse directions (T) (i.e. when the loading direction is inclined or perpendicular to the primary arms of the dendrites), plastic deformation is accompanied by a series of inclined or perpendicular striations that ripple along the gage length of the specimens. This phenomenon is attributed to the growth of stable necks in multiple locations placed within the primary arms of the dendrites and leads to additional strength and capability to withstand plastic deformation beyond necking. The striations are visible on the surface of the specimens (Fig. 6b) and are characterized by the repeated colour patterns of the in-plane strains measured by DIC that are shown in Fig. 7.

In contrast, the longitudinal (L) test specimens disclose a conventional colour pattern typical of localized necking in a single region of the gage length (Fig. 7) because tensile loading is basically elongating the dendrites without creating significant obstruction to the movement of dislocations. The obstruction of dislocations by the primary arms of the dendrites is the main reason why the tensile strength of the deposited AISI 316L is larger than that of the commercial AISI 316L sheets for strains up to 0.2.

Figure 8a presents the strain loading paths and the strains at fracture for the longitudinal (L), inclined (I) and transverse (T) tensile test specimens extracted from the deposited AISI 316L stainless steel. The strain loading paths were obtained by DIC (Sect. 2.1) while the gauge length strains at fracture were determined from individual measurements of thickness along the cracks with an

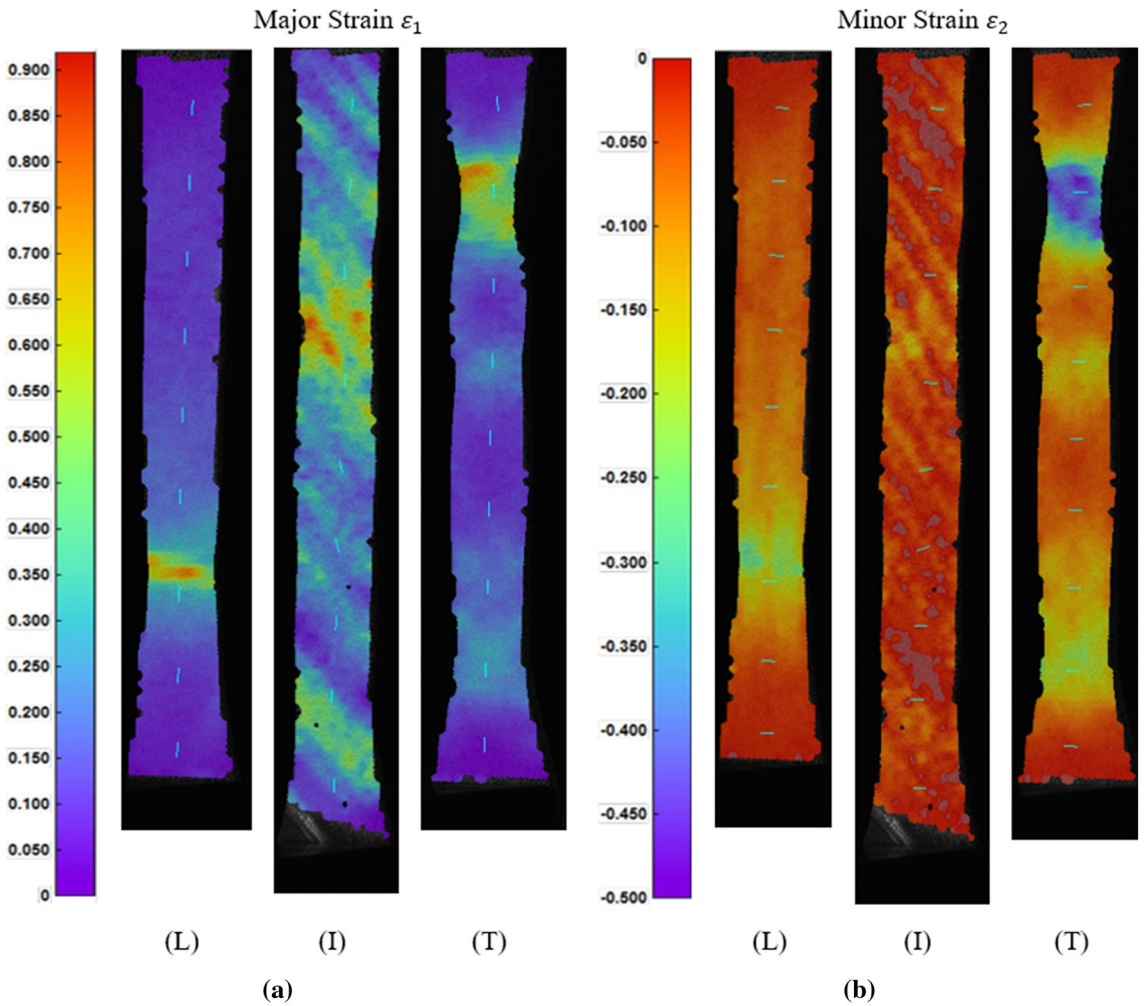


**Fig. 7** Experimental **a** major $\varepsilon_1$ and **b** minor $\varepsilon_2$ in-plane strains obtained by DIC for the longitudinal (L), inclined (I), and transverse (T) test specimens from the deposited AISI 316L stainless steel at the end of tensile testing

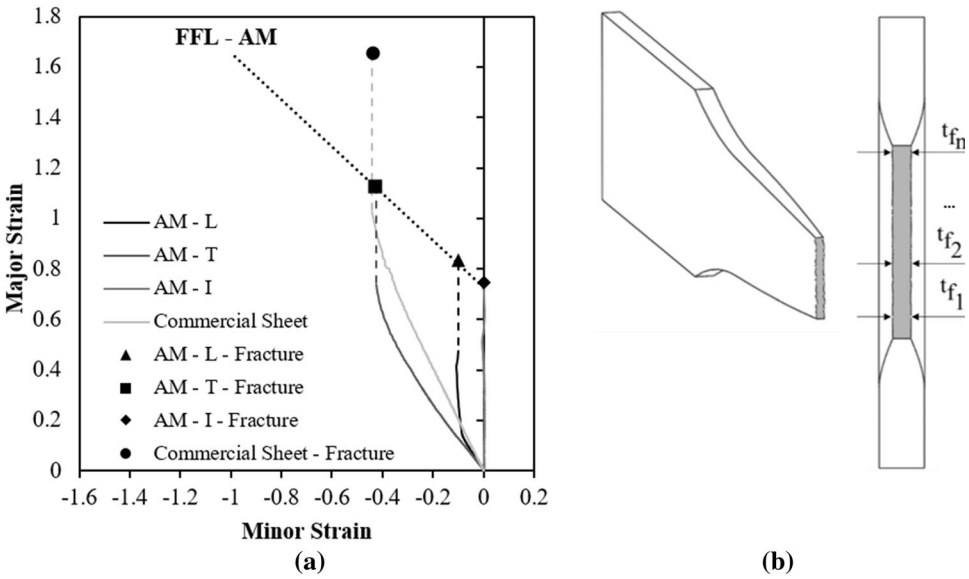


**Fig. 8** Formability of the longitudinal, inclined and transverse tensile test specimens extracted from the deposited AISI 316L stainless steel. **a** Strain loading paths and fracture strains in principal strain space. Results for the commercial AISI 316L sheets are included for comparison purposes; **b** Schematic illustration of the specimen's thickness along the crack

optical microscope Motic model BA310 MET-H with a magnification of 20× [27].

The procedure for determining the gauge length strains at fracture is schematically illustrated in Fig. 8b and the thickness strains along the cracks $\varepsilon_3^f$ are calculated as follows,

$$\varepsilon_3^f = ln\left(\frac{t_f}{t_0}\right) \tag{1}$$

where $t_0$ is the initial thickness and $t_f$ is the average crack thickness of the specimens. The minor strain at fracture $\varepsilon_2^f$ is assumed to remain constant after the last measurement by DIC in order to account for localization under plane strain deformation conditions, while the major strain $\varepsilon_1^f$ is obtained by incompressibility,

$$\varepsilon_1^f = -\left(\varepsilon_2^f + \varepsilon_3^f\right) \tag{2}$$

The resulting gauge length strains at fracture are plotted as solid circular markers in Fig. 8a.

Generally speaking, there are three different behaviours in principal strain space. The strain loading path of the longitudinal (L) test specimens is aligned with the direction of pure tension and the onset of necking is well-defined by the abrupt change in direction towards plane strain deformation.

The strain loading path of the transverse (T) test specimens is located in-between pure tension and pure shear. The onset of necking is not so well-defined because the change in direction towards plane strain deformation occurs progressively due to the growth of stable necks in multiple locations within the primary arms of the dendrites. The resulting major gauge length strain at fracture $\varepsilon_1^f$ is the highest for the three different types of specimens.

The strain loading path of the inclined (I) test specimens evolves under plane strain deformation from the beginning to the end of testing. This is a rather peculiar result for a tensile test that can only be explained by the influence of the dendritic microstructure in the overall plastic deformation.

The straight line with slope − 0.93 connecting the fracture strains of the longitudinal, inclined and transverse test specimens is the fracture forming line (FFL) and corresponds to crack opening by tension (mode I of fracture mechanics). This line will be of paramount importance to analyse the formability of the deposited AISI 316L stainless steel during incremental sheet forming.

To conclude it is worth mentioning that the fracture strains obtained from tensile tests performed with the AISI 316L commercial sheets (Fig. 8a) are approximately 67% higher than those of the deposited material.

## 3.2 Incremental Sheet Forming of the Deposited and Commercial sheets

After comparing the mechanical performance of the deposited AISI 316L stainless steel with that of a commercial sheet and having gained a better understanding on the influence of the deposited material microstructure on formability, it is important to assess the integration of metal forming in hybrid AM systems. This was carried out by analysing the incremental forming of a deposited U-shaped part and by comparing its overall formability with that of a commercial AISI 316L sheet.

Figure 9a shows the evolution of the major and minor true strains along the meridional direction in principal strain space for both the deposited and commercial sheets. The resulting gauge length strains at fracture are plotted as solid circular markers and were obtained by means of the same

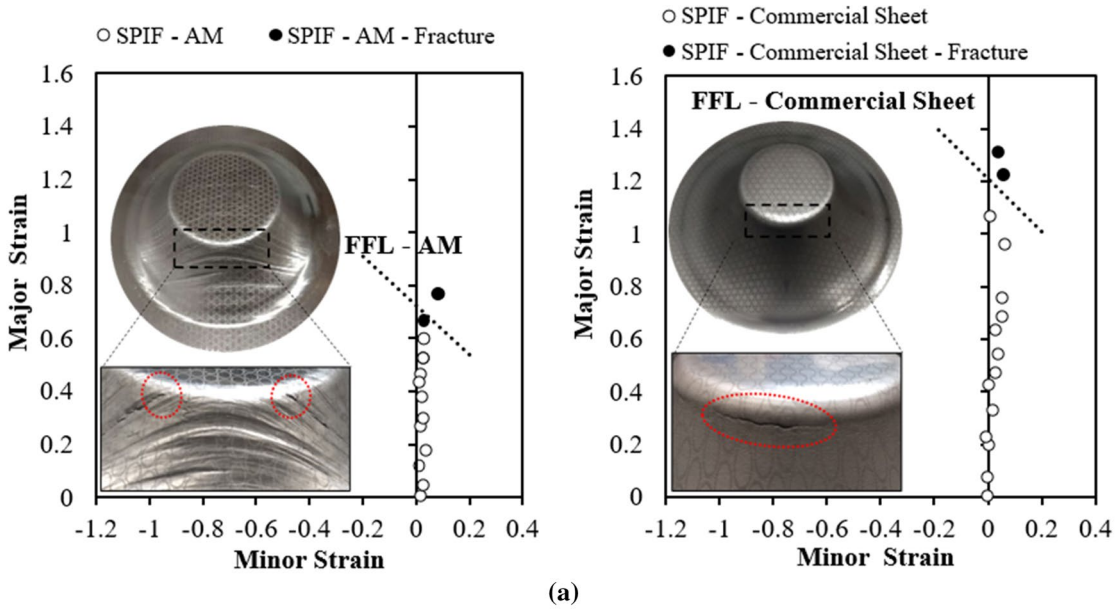


(a)

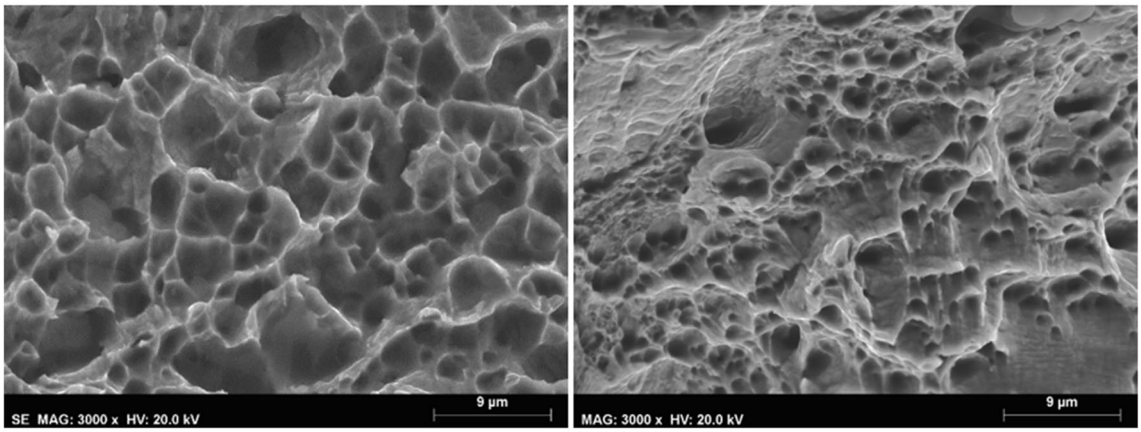


(b)

**Fig. 9** Incremental forming of truncated conical shapes made from deposited (left) and (right) commercial AISI 316L sheets. **a** Major and minor experimental true strains along the meridional direction obtained from circle grid analysis. The solid markers correspond to fracture; **b** Scanning electron microscope (SEM) of the cracked surfaces using a magnification of 3000×. The pictures are representative of the entire length of the cracks

experimental procedure that was utilized in Sect. 3.1 (refer to Fig. 8).

The FFL of the deposited AISI 316L stainless steel was that previously determined in Sect. 3.1 whereas the FFL of the commercial AISI 316L sheet was obtained by taking the corresponding gauge length strains at fracture (refer to the solid circular marker in Fig. 8a) and a theoretical slope of '-1' [26].

Results confirm that the truncated conical shapes are formed under plane strain loading conditions and that gauge length strains at fracture are close to the experimental FFL retrieved from tensile tests with longitudinal, inclined and transverse test specimens (Fig. 8a).

Circle grid analysis (CGA) also reveals that formability of the commercial AISI 316L sheet is significantly higher (approximately 67%) than that of the deposited AISI 316L, allowing to reach major true strains at fracture $\varepsilon_1^f \cong 1.3$. The reason for this difference is not due to changes in the crack opening mechanism, which is by tension in both cases, but to differences in the microstructure of the deposited and commercial AISI 316L stainless steel.

In fact, SEM images of the fracture surfaces retrieved from the two different incrementally formed parts reveal circular dimpled structures (Fig. 9b) typical of crack opening by tension. This observation is in good agreement with the fracture strains being close to the FFL (Fig. 9a) and to failure

being triggered by tension (mode I of fracture mechanics) in both deposited and commercial AISI 316L sheets.

The particularities of the deposited AISI 316L microstructure, namely the existence of dendrites with primary arms aligned with the AM build direction, are once again responsible for the striations that are visible on the side wall of the truncated conical shapes. The striations are attributed to the growth of stable necks within the primary arms of the dendrites and give rise to significant planar anisotropy.

As seen in the photographic detail provided in Fig. 9a (left), cracks are triggered in directions parallel to the striations as these locations are inclined to the loading direction applied to the primary arms of the dendrites. In other words, cracks are triggered in directions compatible with those of the inclined tensile test specimens of Sect. 3.1, which were found to provide the poorer formability results.

The presence of striations also influences the evolution of the wall thickness with depth (Fig. 10a). Generally speaking, the wall thickness decreases with depth, meaning that plastic deformation takes place by thinning until fracture. However, a closer look at Fig. 10a allows identifying two different patterns that are dependent on the location from where the meridional cross-sections were extracted.

The cross-section extracted from a region where striations are visible provide a non-uniform (oscillatory) thinning until fracture whereas the cross-section extracted from a smooth region without striations provide a more uniform thinning until fracture. This difference is visible in the cross-section photographic details of Fig. 10b and c and the non-uniform thinning pattern is attributed to multiple growth of stable necks within the primary arms of the dendrites.

### 3.3 Towards the Fabrication of Complex AM Parts

The choice of incremental forming as a benchmark process to evaluate the potential of hybrid AM systems containing additive, subtractive and forming manufacturing stages was further considered by producing the part shown in Fig. 11. The goal was to fabricate a truncated eight lobe conical shape by incremental forming with a hemispherical-ended

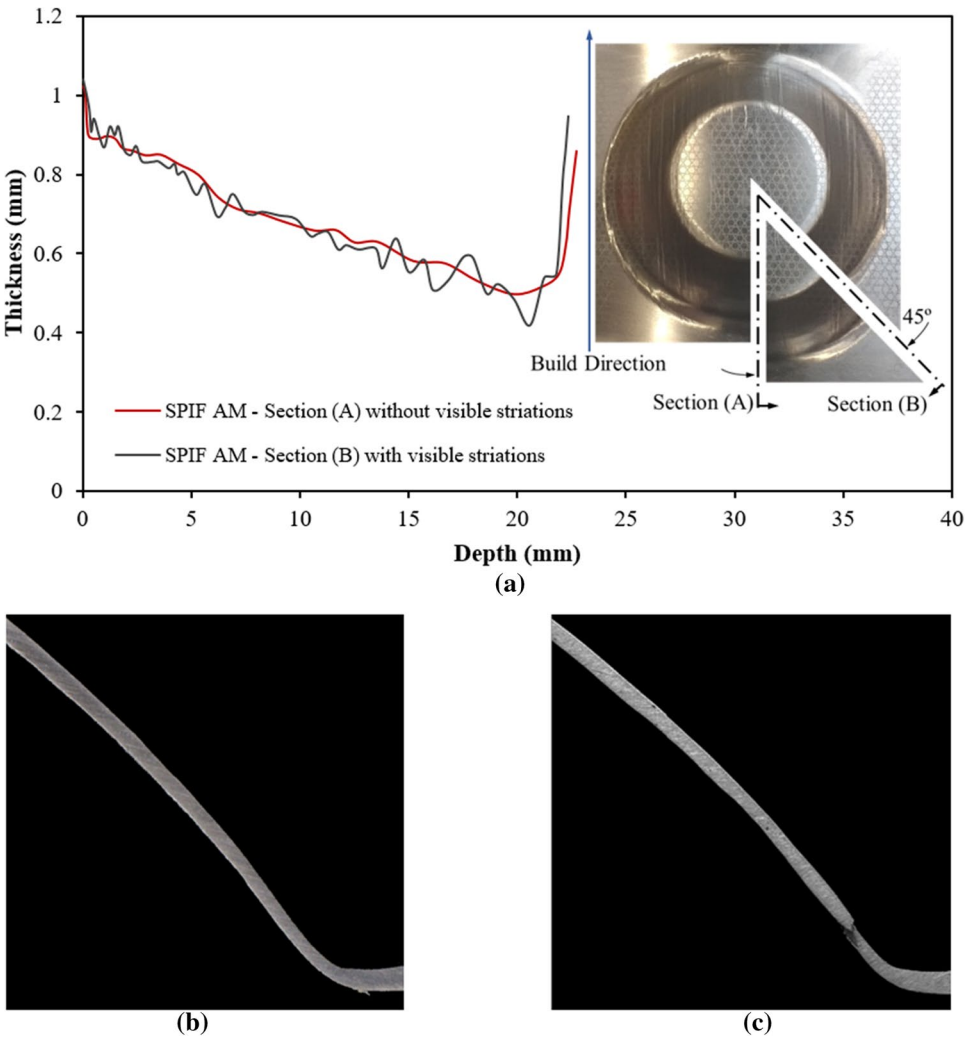


**Fig. 10** Wall thickness variations of the truncated conical shape produced by incremental sheet forming of deposited AISI 316L stainless steel. **a** Variation of wall thickness with depth for two different meridional cross-sections that include and do not include surface striations; **b** Photograph of a meridional cross-section 'A' of a region where striations are not visible; **c** Photograph of a meridional cross-section 'B' of a region where striations and fracture are visible

**Fig. 11** Top and bottom view of a truncated eight lobe conical shape produced by a hybrid processing route comprising metal deposition by WAAM, milling and incremental forming

tool from a deposited U-shaped part of AISI 316L with 130 mm length, 130 mm height and 50 mm side wall width. The as-build U-shaped part was milled in the region to be plastically deformed in order to ensure good surface conditions and a uniform thickness of approximately 1 mm.

The fabrication of a similar part in a hybrid AM system solely having additive and subtractive manufacturing capabilities would not only require a significant amount of extra material to be deposited, and subsequently machined out to obtain the desired shape, as it would raise difficulties in machining due to the small thickness and sharp concave corners of the truncated eight lobe conical shape.

Another advantage of the deposited U-shaped geometry is the artificial constraint provided by its baseplate and the side walls, which allow forming the required shape without using a backing plate and a blank holder. The utilization of these tool components is mandatory in conventional incremental forming of commercial sheets.

The above conclusion is relevant because it means that incremental forming can be directly performed on top of the post-processed regions of the deposited material without extra tool requirements. This shortens the overall processing time and enhances the flexibility to produce complex AM ready-to-use parts.

## 4 Conclusions

The integration of forming operations on hybrid additive manufacturing (AM) systems based on WAAM allows changing the shape and alter the surface of the as-build deposited parts while keeping its volume constant. The flexibility of the resulting hybrid AM systems increases and its applicability can be extended to the fabrication of complex ready-to-use parts that would be impossible or significantly more costly and time consuming to be produced in conventional AM systems.

Microstructural and scanning electron microscope (SEM) observations combined with determination of the strain loading paths by digital image correlation (DIC) and circle grid analysis (CGA), and evaluation of the gauge length strains at fracture allow concluding that formability of deposited AISI 316L stainless steel is smaller than that of commercial sheets made from the same material. However, despite formability being smaller (with major principal true strains reduced by approximately 67%) it is still appropriate to withstand large plastic deformations that are typical of metal forming.

The deposited AISI 316L stainless steel is strongly anisotropic due to the dendritic based microstructure resulting from the temperature gradient perpendicular to the reciprocated single bead layers of the deposited part. The growth of stable necks within the primary arms of the dendrites gives rise to striations that ripple along the gage length of the tensile test specimens and the side wall of the truncated conical shapes produced by incremental forming whenever loading conditions are inclined or perpendicular to the primary arms of the dendrites. The striations are visible on the surfaces and cross-section thickness measurements disclose oscillatory values that are typical of multiple stable neck growth.

Loading in directions inclined to the primary arms of the dendrites gives rise to plane strain deformation conditions and to the lowest values of the gauge length strains at the onset of fracture. This justifies the reason why cracks were triggered along this direction during incremental forming of the truncated conical shapes made from the deposited AISI 316L stainless steel.

**Acknowledgements** The authors would like to acknowledge the support provided by Fundação para a Ciência e a Tecnologia of Portugal and IDMEC under LAETA-UID/EMS/50022/2019. Valentino Cristino would like to acknowledge the support provided by the Science and Technology Development Fund of Macao (Grant no. 164/2017/A).

### Compliance with ethical standards

**Conflict of interest** The authors state that there is no conflict of interest.

## References


1. Merklein, M., Junker, D., Schaub, A., & Neubauer, F. (2016). Hybrid additive manufacturing technologies–an analysis regarding potentials and applications. *Physics Procedia*. https://doi.org/10.1016/j.phpro.2016.08.057.
2. Lu, X., Zhou, Y. F., Xing, X. L., Shao, L. Y., Yang, Q. X., & Gao, S. Y. (2017). Open-source wire and arc additive manufacturing system: Formability, microstructures, and mechanical properties. *The International Journal of Advanced Manufacturing Technology*. https://doi.org/10.1007/s00170-017-0636-z.
3. Yi, H., Qi, L., Luo, J., Zhang, D., Li, H., & Hou, X. (2018). Effect of the surface morphology of solidified droplet on remelting between neighbouring aluminum droplets. *International Journal of Machine Tools and Manufacture*. https://doi.org/10.1016/j.ijmachtools.2018.03.006.
4. Yi, H., Qi, L., Luo, J., Zhang, D., & Li, N. (2019). Direct fabrication of metal tubes with high-quality inner surfaces via droplet deposition over soluble cores. *Journal of Materials Processing Technology*. https://doi.org/10.1016/j.jmatprotec.2018.09.004.
5. Donoghue, J., Antonysamy, A. A., Martina, F., Colegrove, P. A., Williams, S. W., & Prangnell, P. B. (2016). The effectiveness of combining rolling deformation with Wire-Arc Additive Manufacture on β-grain refinement and texture modification in Ti–6Al–4 V. *Materials Characterization*. https://doi.org/10.1016/j.matchar.2016.02.001.
6. Butzhammer, L., Dubjella, P., Huber, F., Schaub, A., Aumüller, M., Baum, A., Petrunenko, O., Merklein, M., & Schmidt, M. (2017). Experimental investigation of a process chain combining sheet metal bending and laser beam melting of Ti-6Al-4 V. In L. Overmeyer, U. Reisgen, A. Ostendorf, M. Schmidt (Ed.), *Proceedings of the Lasers in Manufacturing Conference* (pp. 26–29). Munich: LIM.
7. Bambach, M. D., Bambach, M., Sviridov, A., & Weiss, S. (2017). New process chains involving additive manufacturing and metal forming–a chance for saving energy? *Procedia Engineering*. https://doi.org/10.1016/j.proeng.2017.10.1049.
8. Yoon, H. S., Lee, J. Y., Kim, H. S., Kim, M. S., Kim, E. S., Shin, Y. J., et al. (2014). A comparison of energy consumption in bulk forming, subtractive, and additive processes: Review and case study. *International Journal of Precision Engineering and Manufacturing-Green Technology*. https://doi.org/10.1007/s40684-014-0033-0.
9. Zhu, Z., Dhokia, V. G., Nassehi, A., & Newman, S. T. (2013). A review of hybrid manufacturing processes–state of the art and future perspectives. *International Journal of Computer Integrated Manufacturing*. https://doi.org/10.1080/0951192X.2012.749530.
10. Karunakaran, K. P., Suryakumar, S., Pushpa, V., & Akula, S. (2010). Low cost integration of additive and subtractive processes for hybrid layered manufacturing. *Robotics and Computer-Integrated Manufacturing*. https://doi.org/10.1016/j.rcim.2010.03.008.
11. Hölker, R., Jäger, A., Ben Khalifa, N., & Tekkaya, A.E. (2014). Process and apparatus for the combined manufacturing of workpieces by incremental sheet metal forming and manufacturing methods in one set-up. *German Patent Application*. DE 10 2014 014 202.7.
12. Papke, T., Junker, D., Schmidt, M., Kolb, T., & Merklein, M. (2018). Bulk metal forming of additively manufactured elements. *MATEC Web of Conferences*. https://doi.org/10.1051/matecconf/201819003002.
13. Ahuja, B., Schaub, A., Karg, M., Schmidt, R., Merklein, M., & Schmidt, M. (2015). High power laser beam melting of Ti-6Al-4V on formed sheet metal to achieve hybrid structures. *Laser 3D Manufacturing II*. https://doi.org/10.1117/12.2082919.
14. Ambrogio, G., Gagliardi, F., Muzzupappa, M., & Filice, L. (2019). Additive-incremental forming hybrid manufacturing technique to improve customised part performance. *Journal of Manufacturing Processes*. https://doi.org/10.1016/j.jmapro.2018.12.008.
15. Bambach, M., Sviridov, A., Weisheit, A., & Schleifenbaum, J. (2017). Case studies on local reinforcement of sheet metal components by laser additive manufacturing. *Metals*. https://doi.org/10.3390/met7040113.
16. Shirizly, A., & Dolev, O. (2019). From wire to seamless flow-formed tube: leveraging the combination of wire arc additive manufacturing and metal forming. *JOM Journal of the Minerals Metals and Materials Society*. https://doi.org/10.1007/s11837-018-3200-x.
17. Silva, D.F., Bragança, I.M.F., Silva, C.M.A., Alves, L.M., & Martins, P.A.F. (2019). Joining by forming of additive manufactured 'mortise-and-tenon'joints. *Proceedings of the Institution of Mechanical Engineers, Part B: Journal of Engineering Manufacture*. https://doi.org/10.1177/0954405417720954.
18. Wu, B., Pan, Z., Ding, D., Cuiuri, D., Li, H., Xu, J., et al. (2018). A review of the wire arc additive manufacturing of metals: Properties, defects and quality improvement. *Journal of Manufacturing Processes*. https://doi.org/10.1016/j.jmapro.2018.08.001.
19. Jackson, M. A., Van Asten, A., Morrow, J. D., Min, S., & Pfefferkorn, F. E. (2018). Energy consumption model for additive-subtractive manufacturing processes with case study. *International Journal of Precision Engineering and Manufacturing-Green Technology*. https://doi.org/10.1007/s40684-018-0049-y.
20. Campatelli, G., Montevecchi, F., Venturini, G., Ingarao, G., & Priarone, P. C. (2019). Integrated WAAM-subtractive versus pure subtractive manufacturing approaches: an energy efficiency comparison. *International Journal of Precision Engineering and Manufacturing-Green Technology*. https://doi.org/10.1007/s40684-019-00071-y.
21. Yang, D. Y., Bambach, M., Cao, J., Duflou, J., Groche, P., Kuboki, T., et al. (2018). Flexibility in metal forming. *CIRP Annals*. https://doi.org/10.1016/j.cirp.2018.05.004.
22. Silva, C. M. A., Bragança, I. M. F., Cabrita, A., Quintino, L., & Martins, P. A. F. (2017). Formability of a wire arc deposited aluminium alloy. *Journal of the Brazilian Society of Mechanical Sciences and Engineering*. https://doi.org/10.1007/s40430-017-0864-z.
23. Rosenthal, S., Platt, S., Hölker-Jäger, R., Gies, S., Kleszczynski, S., Tekkaya, A. E., et al. (2019). Forming properties of additively manufactured monolithic Hastelloy X sheets. *Materials Science and Engineering A*. https://doi.org/10.1016/j.msea.2019.03.035.
24. López, C., Elías-Zúñiga, A., Jiménez, I., Martínez-Romero, O., Siller, H., & Diabb, J. M. (2018). Experimental determination of residual stresses generated by single point incremental forming of AlSi10 Mg sheets produced using SLM additive manufacturing process. *Materials*. https://doi.org/10.3390/ma11122542.
25. ASTM E8/E8 M (2016) *Standard Test Methods for Tension Testing of Metallic Materials*. West Conshohocken: ASTM International.
26. Silva, M. B., Skjoedt, M., Atkins, A. G., Bay, N., & Martins, P. A. F. (2008). Single point incremental forming & formability/failure diagrams. *Journal of Strain Analysis for Engineering Design*. https://doi.org/10.1243/03093247JSA340.
27. Magrinho, J.P., Silva, M.B., Reis, L., & Martins, P.A.F. (2019). Formability Limits, Fractography and Fracture Toughness in Sheet Metal Forming. *Materials*. https://doi.org/10.3390/ma12091493.
28. Wu, W., Xue, J., Wang, L., Zhang, Z., Hu, Y., & Dong, C. (2019). Forming process, microstructure, and mechanical properties of thin-walled 316L stainless steel using speed-cold-welding additive manufacturing. *Metals*. https://doi.org/10.3390/met9010109.

**João P. M. Pragana** is PhD student of Mechanical Engineering at Instituto Superior Técnico University of Lisbon, Portugal. He obtained a MSc in Mechanical Engineering from Instituto Superior Técnico in 2017, where he also served as junior researcher between 2017 and 2018 of the Manufacturing and Industrial Management Unit. His current research focus is on metal forming, joining technologies and additive manufacturing.

**Valentino A. M. Cristino** is assistant professor of the Department of Electromechanical Engineering of University of Macau (China). He received his PhD in Mechanical Engineering from Instituto Superior Técnico, University of Lisbon, Portugal, in 2012, where he also worked previously as the Facility Engineer of the laboratory infrastructure of the Manufacturing and Industrial Management Unit between the years 2004 to 2013. His research interests are focused in metal forming and metal cutting.

**Ivo M. F. Bragança** obtained his PhD in Mechanical Engineering from Instituto Superior Técnico, Universidade de Lisboa, in 2013 and he is currently invited assistant professor at Instituto Superior Engenharia de Lisboa, Instituto Politécnico de Lisboa. His research interests include non-traditional processes, joining by plastic deformation and more recently additive manufacturing. He is an Integrated Member of the Associated Laboratory for Energy, Transports and Aeronautics.

**Carlos M. A. Silva** is assistant professor at Instituto Superior Técnico, University of Lisbon, Portugal. He obtained a PhD in Mechanical Engineering from Instituto Superior Técnico in 2013. He is an Integrated Member of the Associated Laboratory for Energy, Transports and Aeronautic and, between 2013 and 2015, he served as Facility Engineer for the laboratory infrastructure of the Manufacturing and Industrial Management Unit of Instituto Superior Técnico. He was invited assistant professor at the Faculty of Engineering of Catholic University of Portugal in 2013. His research interests are focused in metal forming, joining technologies and additive manufacturing.

**Paulo A. F. Martins** is professor of manufacturing at Instituto Superior Técnico, University of Lisbon, Portugal. He obtained a PhD in mechanical engineering from Instituto Superior Técnico in 1991, the habilitation in mechanical engineering from Instituto Superior Técnico in 1999 and the degree of doctor technices honoris causa from the Technical University of Denmark in 2018. He was president of the scientific board at Instituto Superior Técnico from 2009 to 2012 and he is president of the school council of Instituto Superior Técnico since 2017. His research interests are focused in metal forming and joining technologies.